Spiral wave dynamics in excitable media with spherical geometries

Katrin Rohlf
Department of Mathematics, Ryerson University, 350 Victoria Street, Toronto, Ontario M5B 2K3, Canada

Leon Glass
Department of Physiology, McGill University, 3655 Promenade Sir William Osler, Montreal, Quebec H3G 1Y6, Canada

Raymond Kapral
Chemical Physics Theory Group, Department of Chemistry, University of Toronto, Toronto, Ontario M5S 3H6, Canada

(Received 15 June 2006; accepted 8 August 2006; published online 27 September 2006)

We describe the spatial and temporal organization of spiral and scroll waves in spherical shells of different sizes and solid spheres. We present simulation results for the evolution of the dynamics and clustering of spiral waves as a function of the excitability of the medium. The excitability, topology, and size of the domain places restrictions on how single and multiarmed spiral waves are organized in space. The results in spherical geometries are compared with those in planar two-dimensional media. These studies are relevant to the dynamics of spiral waves in a variety of media including the heart, and chemical reactions on spherical surfaces. © *2006 American Institute of Physics*. [DOI: 10.1063/1.2346237]

Reentrant activity in the form of spiral or scroll waves plays a fundamental role in a wide range of physical, chemical, and biological systems. In the case of heart tissue, interaction, and self-organization of spiral waves may be of interest, particularly in three-dimensional geometries. Following a brief survey of some general properties pertaining to motion of isolated singularities in three-dimensional geometries, we explore the self-organization of many singularities as a function of medium properties and geometry. Our results indicate that although there are some common features in the self-organization of singularities in two-dimensional and three-dimensional geometries, some important differences arise in weakly excitable media.

I. INTRODUCTION

The existence of spiral or scroll waves has been well documented for a wide range of physical, chemical, and biological systems.[1] Spiral waves in chemical systems have been studied extensively[2] in the Belousov-Zhabotinsky reaction[3,4] and surface catalytic oxidation reactions.[5] In biological systems they play a role in the cAMP waves in dictyostelium discoideum[6] and Ca^{+2} waves in pancreatic β cells,[7] to cite just a few examples. They are also involved in electrical wave propagation in cardiac tissue.[8–10] Spiral waves can break up under certain conditions leading to irregular spatio-temporal patterns that may be responsible for cardiac fibrillation.[11,12] In such circumstances it is convenient to focus on counting the numbers and chiralities of spiral waves that characterize the spatio-temporal pattern.[13] Multiarmed spirals may also occur, and such patterns have been observed experimentally in the Belousov-Zhabotinsky reaction,[14] mounds of dictyostelium discoideum,[15] and two-dimensional cardiac cultures.[16]

A variety of factors can influence the dynamics of spiral waves. These include external fields[17–20] and spatial inhomogeneities.[21–26] The excitability of the medium is also an important factor in determining the nature and dynamics of the spiral waves. In media with reduced excitability where isolated spirals have a core, spiral interactions play a more dominant role. For two-dimensional sheets with no-flux boundary conditions, spiral interactions lead to induced migration of spiral waves with elimination of many spiral waves through collisions with the boundaries of the medium, or each other. On large sheets after long simulation times,[27] or on smaller sheets,[15] surviving spiral waves group together forming self-organized states in the form of multiarmed spirals. In finite circular domains, it has been shown that in some cases the interaction of spirals with medium boundaries leads to drift of the spirals along the boundary,[28] and if the circular domain is small enough, the frequency of rotation may increase substantially.[29]

It has long been recognized that geometry can influence the nature and dynamics of spiral waves. For instance, cardiac tissue is inhomogeneous and the heart is a thick excitable medium with a complex nonplanar geometry. These features influence the dynamics of cardiac electrochemical waves and must be incorporated in realistic heart models.[9,10,30–32] However, by examining model systems with simple geometries, we can help clarify the ways in which geometry interacts with dynamics. The spherical geometry is one of the simplest contexts in which to investigate the effects of curvature and, more generally, geometry, on spiral dynamics and both theory and simulation have been used to explore spiral dynamics in such systems.[21,33]

This paper is organized as follows: In Sec. II we present a brief survey of spiral wave dynamics on spherical surfaces and point out some of its distinctive features in comparison

to the analogous behavior on planar media with given boundary conditions. Boundary effects do not play a role on spherical surfaces and this places restrictions on the nature and numbers of spiral waves that can exist in the system. Section III presents results for the dynamics of spiral waves on spherical surfaces when the excitability of the medium varies. In this section we show that multiarmed spirals form on the spherical surface as the excitability of the medium decreases and these clusters form and evolve in characteristic ways that depend on the geometry. We compare these results with similar studies on planar geometries. Scroll wave filament dynamics in thick spherical shells and solid spheres is briefly reviewed in Sec. IV where again the spherical geometry plays a role in determining the dynamics.

II. SPIRAL WAVES ON SPHERICAL SURFACES

In this section we review some aspects of the dynamics of spiral waves on spherical surfaces or spherical shells of excitable media that are sufficiently thin so that the medium is effectively two-dimensional. In comparison to spiral wave dynamics on planar geometries, the consideration of spherical geometries introduces new features since spiral waves cannot collide with boundaries, and the geometry places topological restrictions on the numbers and chiralities of the spiral waves. In addition, the curvature of the surface leads to spiral wave motion that differs from that in planar media.

Excitable media are typically described in terms of reaction-diffusion models with propagator-controller (or activator-inhibitor) kinetics which take the general form,

$$\frac{\partial u(\mathbf{r},t)}{\partial t} = R_u(u,v) + D_u \nabla^2 u,$$
$$\frac{\partial v(\mathbf{r},t)}{\partial t} = R_v(u,v) + D_v \nabla^2 v. \tag{1}$$

Here u is the propagator with an N-shaped nullcline, $R_u(u,v)=0$, and v is the controller variable with a monotonic nullcline, $R_v(u,v)=0$. The diffusion coefficients of these species are D_u and D_v, respectively. A prototypical example of a excitable media is the FitzHugh-Nagumo (FHN) model,[34–36] where

$$R_u(u,v) = -ku(u-a)(u-1) - lv,$$
$$R_v(u,v) = (u-v)/\tau. \tag{2}$$

Provided $|a-1| < 2\sqrt{l/k}$ there is a unique stable fixed point at the origin. We shall use this FHN model to illustrate the results in this paper.

Rotating spiral waves in two dimensions can be characterized by an index, and restrictions on the numbers and types of spiral waves are provided by an index theorem. With the exception of a finite number of singular points (located at the "tips" of spiral waves), each point in an orientable and compact two-dimensional differentiable manifold M is assigned a unique phase Φ.[39] The resulting phase field is assumed to be continuously differentiable except at the singular points. Given any positively oriented closed curve C that does not pass through a singularity in a two-dimensional phase field, one can compute the index I of the curve (also called the winding number, topological charge,[40] or topological defect) using the line integral

$$2\pi I = \oint_C \nabla \Phi \cdot d\mathbf{l}. \tag{3}$$

Phase singularities will lead to nonzero integer indices for curves encircling the singularities. In our case, the two-dimensional domain is a thin spherical shell of fixed radius, and C is any curve on its surface.[41] If more than one singularity is located inside C, then I is the sum of the indices of each of the singularities. If the curve C is small enough, nonzero values of the integral indicate existence of a singularity inside C, or in our case, existence of a spiral tip or multiarmed spiral on the spherical surface. The sum of the indices of all singular points is zero for oriented two-dimensional surfaces.[42] The implication of this result is that the numbers and types of singularities are restricted. For example, if all singularities have an index of ± 1, then singularities must occur in pairs of opposite sign on spherical shells so that the sum of the indices is zero. The existence of holes in the geometry does not affect this result provided the domain is connected, and one determines the index of holes by considering a closed curve C encompassing the hole.[21]

On a curved surface the reaction-diffusion equation takes the form[43]

$$\frac{\partial u(\mathbf{x},t)}{\partial t} = R_u(u,v) + D_u \frac{1}{\sqrt{g}} \frac{\partial}{\partial x^\alpha}\left(g^{\alpha\beta}\sqrt{g}\frac{\partial}{\partial x^\beta}\right) u,$$
$$\frac{\partial v(\mathbf{x},t)}{\partial t} = R_v(u,v) + D_v \frac{1}{\sqrt{g}} \frac{\partial}{\partial x^\alpha}\left(g^{\alpha\beta}\sqrt{g}\frac{\partial}{\partial x^\beta}\right) v. \tag{4}$$

Here $g_{\alpha\beta}$ is the metric tensor and g is its determinant. Approximate spiral wave solutions of this equation for homogeneous excitable media have been constructed using kinematic theory for weakly excitable media where the pitch of the spiral wave is much larger than the length of the refractory zone following the excitation. In this circumstance the spiral wave can be approximated as a space curve with length ℓ parameterized by the arc length s, with a free end at $s=0$, and characterized by the local geodesic curvature $\kappa(s)$. In the case where the inhibitor is immobilized ($D_v=0$), one can make use of the eikonal relations connecting the normal velocity v_N of the front to the curvature and planar velocity v_p, $v_N = v_p - D_u\kappa$ (Ref. 44) with the analogous equation for the tangential front velocity at the free end of the space curve, $v_{Tf} = v_{Tfp} - \gamma_f \kappa(0)$, leading to the equation of motion for the local curvature[47,48]

$$\frac{\partial}{\partial t}\kappa(s,t) = -\frac{\partial^2 v_N}{\partial s^2} - \kappa^2 v_N - \frac{\partial \kappa}{\partial s}\left(\int_0^s ds' \kappa(s',t) v_N + v_{Tf}\right) - \Gamma v_N, \tag{5}$$

where $\Gamma = 1/R^2$ is the Gaussian curvature of the sphere. Solutions of this equation for a steadily rotating spiral wave on the surface of a sphere have been constructed.[47–50] In this case Eq. (5) admits two solutions which are symmetric and antisymmetric with respect to the sphere equator. Only the

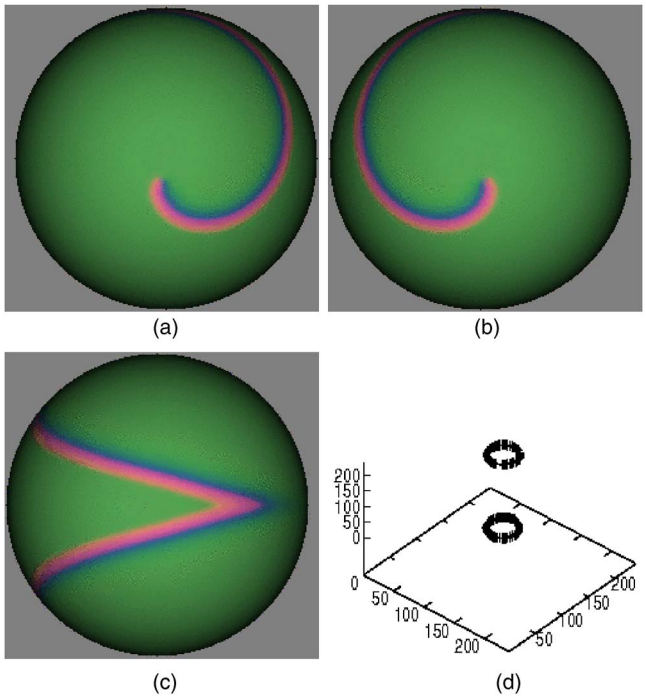

FIG. 1. (Color online) Symmetric spiral solution on a sphere. Top (a), bottom (b), and side (c) views of the sphere. Also shown in (d) is the time evolution of the spiral tip locations when $\tau=5$.

symmetric solution is allowed on the sphere surface in view of the structure of Eq. (5) under the transformation $s \rightarrow \ell - s$. Figure 1 shows such a symmetric solution obtained in a simulation of the FHN equation for low excitability. The lower right panel of this figure shows that the spiral tips execute circular orbits on the sphere surface.

Kinematic theory also provides an expression for the rotation frequency of the spiral,

$$\omega = \omega_p \left(1 + \frac{v_p \Gamma}{2\xi^2 \gamma \kappa_c^3} \right), \tag{6}$$

where $\kappa_c = v_{Tfp}/\gamma_f$, ω_p is the planar rotation frequency and the numerical factor $\xi=0.685$. This formula predicts that a spiral wave rotates faster on the surface of a sphere than in a planar geometry.

If the excitable medium is inhomogeneous, for example, as a result of the excitability being nonuniform on the surface of the sphere, the spiral waves can now drift on the surface of the sphere.[43] Kinematic theory has been used to predict the existence of such a drift and the fact that the direction of the drift due to gradients depends on the model system and its parameters.[48] In the kinematic description for spiral waves on curved surfaces, only surfaces with nonconstant Gaussian surfaces can lead to drift of spiral tips across the surface.[51] Experimental and theoretical studies show that spiral waves travel to the "top" of a paraboloid or prolate ellipsoid, and the rotation frequency of the spiral is higher on such surfaces than on the plane.[43] The propagation of wave fronts on periodically modulated curved surfaces can also be predicted with the kinematic theory, and the numerical results agree well with experimental findings.[52]

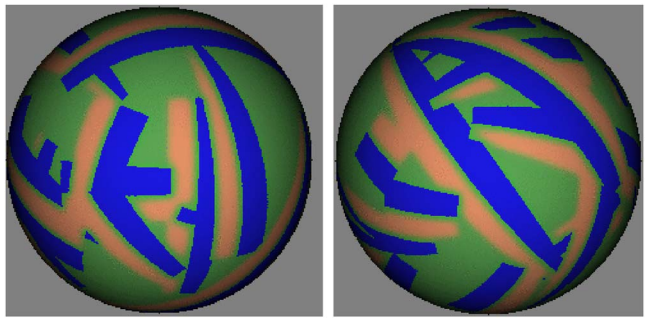

FIG. 2. (Color online) Example of a random initial condition on a thin spherical shell whose outer radius is $R=60$. The two panels show two different views of the sphere with 30 initial segments. Red (or black) regions represent excited domains, blue (or light gray) refractory domains, and green (or dark gray) regions are cells at rest.

Simulations on the FHN model with a linear gradient in the excitability at an angle ϕ to the polar axis illustrates the dynamics of a pair of spirals with opposite chirality initially located near the poles on the sphere.[21] In the presence of a gradient, the frequencies of the two spirals differ and the spiral with the higher frequency controls the dynamics.[53] As a consequence, the low-frequency spiral core is pushed farther from the high-frequency spiral core[53,54] leading to the creation of a source-sink pair.[55] Maselko and Showalter[56,57] observed such source-sink pairs in experiments on the excitable Belousov-Zhabotinsky reaction on spherical beads. However, topological constraints imposed by the index theorem, must nevertheless be satisfied by the source-sink pair.[21] The inhomogeneous excitability also induces a drift of the spiral cores.[21,58] The dominating spiral drifts toward lower excitability and its wave fronts continuously push the other core in the opposite direction. After a long transient the slaved spiral reverses its drift direction and both spirals drift toward lower excitability until they form a stable bound pair. The bound pair slowly moves along a (closed) equiexcitability curve on the surface of the sphere. This example illustrates the complex dynamics that arise from the interplay between inhomogeneity and spherical geometry.

III. EXCITABILITY AND THE DYNAMICS OF SPIRAL WAVES

A. Dynamics on spherical shells

We now consider the dynamics of spiral waves on spherical shells starting from random initial conditions. Our primary focus will be on the nature and dynamics of the spiral waves as a function of the excitability of the medium. The excitability of the medium with FHN kinetics can be tuned conveniently by varying the parameter τ, as discussed in the Appendix. Initial conditions of the form shown in Fig. 2 were employed in this investigation. The phase space trajectory of an excitable system can be partitioned into excitable, refractory and resting (stable state) segments.

The initial conditions comprise randomly oriented segments of refractory domains adjacent to excited domains in a background of the resting state as shown in the figure. All simulations were carried out using algorithms described elsewhere.[59,60]

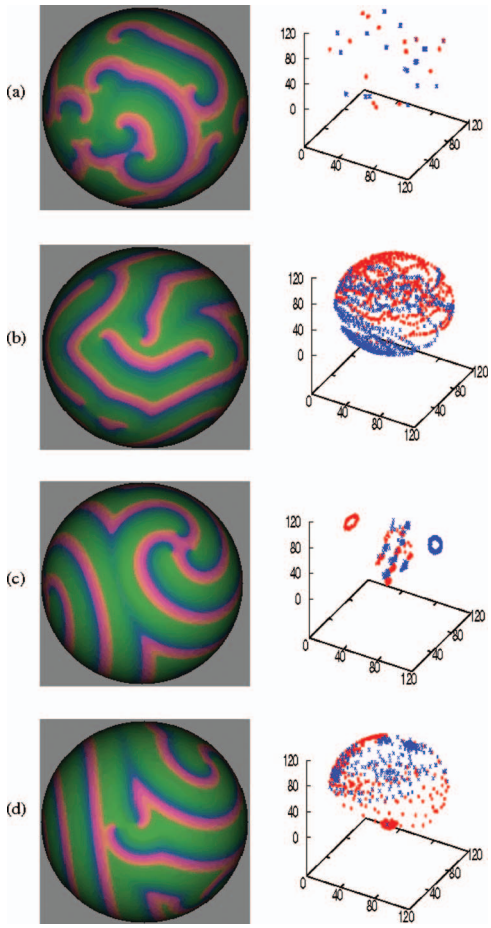

FIG. 3. (Color) Snapshots of spiral waves on spherical shells with $R=60$ for various values of τ (panels on left) and plots of the locations of the singularities every 100 time steps during a time interval of length 5000 (panels on right). Red circles represent locations of the singularities with $I=-1$, while blue crosses are used for $I=+1$. (a) $\tau=10$ with a right view of the sphere (left panel) and singularity dynamics during $25\,000<t<30\,000$. (b) $\tau=8$ with a right view of the sphere and singularity dynamics for $25\,000<t<30\,000$. (c) $\tau=7$ with a top view of the sphere and locations of singularities for $25\,000<t<30\,000$. (d) $\tau=6$ with a top view of the sphere and location of the singularities for $30\,000<t<35\,000$.

An earlier study[33] of excitable FHN kinetics on thin spherical shells showed that, starting from random initial conditions, the system evolved to a random distribution of essentially fixed spiral waves. There was a maximum spiral density, and a minimum spherical shell size was required to support self-sustained spiral waves. Here we consider how the dynamics changes with medium excitability by varying τ. For the rest of this paper, we will refer to a medium as "weakly excitable" if the dynamics of the spiral tip corresponds to motion of waves in a weakly excitable medium (see, for example, Fig. 1 for $\tau=5$) while increasing τ leads to changes in the wave dynamics that generally correspond to an increase in the excitability of a medium. The terminology is rather loose and is discussed more fully in the Appendix.

Figure 3 shows the time evolution of singularities on a spherical shell with $R=60$ for various values of τ (right-hand panels of the figure), together with snapshots of the spiral waves on the sphere taken near the end of the corresponding time interval (left-hand panels). For comparison purposes, in a time interval of length 5000, an isolated singularity would have rotated approximately 50 times for $\tau=5$, 100 times for $\tau=6$, and more than 200 times for $\tau\geq 7$.

For $\tau=10$, many singularities execute small movement across the sphere surface initially ($0\leq t\leq 5000$), but most of the singularities become fixed for later times. Only three out of the thirty singularities exhibit small motion for $5000\leq t\leq 10\,000$, and in particular one singularity moves in a small circular path until about $t\approx 25\,000$. The final state of the system (top row of Fig. 3) is reached when $t\approx 25\,000$. The figure shows the right view of the sphere [Fig. 3(a), left panel] at the end of the time interval $25\,000<t<30\,000$, together with the locations of the singularities found at every 100th time step during this interval [Fig. 3(a), right panel]. All singularities with $I=-1$ (red circles) and $I=+1$ (blue crosses) are stationary during the entire time interval. No clustering of singularities based on index, nor other forms of self-organization were observed.

For $\tau=8$, the system had not reached a steady-state by the time simulations were stopped at $t\approx 30\,000$, and singularities in this transient regime executed extensive motion across the sphere surface. This motion is captured in the singularity plot for $25\,000<t<30\,000$ [right panel of Fig. 3(b)]. In this realization of the dynamics, the singularities perform relatively small motions across the sphere for $0<t<10\,000$, but after this time, singularities move extensively on the sphere surface. The result of this motion is the separation of singularities to opposite hemispheres based on their index. This separation is shown in the second row, right panel of the figure where all $I=-1$ (red circles) singularities are located on the back of the sphere while $I=+1$ (blue crosses) singularities are located on the front.

For $\tau=7$ [Fig. 3(c)], singularities exhibit large-scale motion across the sphere surface, even for $0<t<5000$, and a three-armed spiral, characterized by a cluster of three singularities with the same index, forms during $10\,000<t<15\,000$. During $15\,000<t<20\,000$ a second three-armed spiral forms on the opposite hemisphere. Once this three-armed spiral is formed it induces motion in the first cluster until it becomes fixed once again during $25\,000<t<30\,000$. The final configuration is shown in the third row, left panel of the figure where one of the three-armed spirals that is located on the back right portion of the sphere is clearly visible. Although not completely clear in the picture, the waves on the left hand portion of this view correspond to the waves coming from the second three-armed spiral that resides on the front-left portion of the sphere. The fixed circles in the right-hand panel of Fig. 3(c) represent the time-evolution of the three-armed spirals for $25\,000<t<30\,000$. The red circles correspond to the motion of the three $I=+1$ singularities that make up this three-armed spiral, and the blue circle corresponds to the three-armed spiral comprised of $I=-1$ singularities on the back-right portion of the sphere. The remaining singularities that appear in the graph correspond to isolated singularities on the front-right of the sphere, which are in close proximity to one another, but do not arrange themselves into multiarmed structures.

For $\tau=6$ [Fig. 3(d)], simulations were carried out until $t\approx 35\,000$. A snapshot at the final time of the spherical sur-

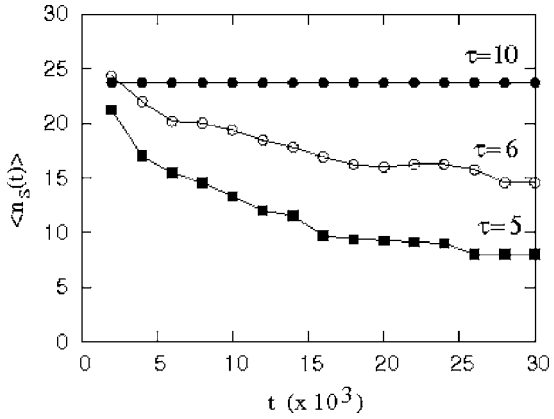

FIG. 4. Plots of the average number of singularities $\langle n_s(t)\rangle$ as a function of time for spherical shells with $R=60$ for various values of τ. See text for details.

face (top view) is shown in the left panel. The two-armed spirals visible in the center of this view correspond to the blue cluster on the center-left portion of the singularity plot in the right panel, which shows the time evolution for $30\,000<t<35\,000$. Other two-armed spirals have formed, but the system is still in the transient regime, although separation of singularities based on charge has occurred in this case as well. As the system evolved in time, a pair of two-armed clusters was visible during $5000<t<10\,000$, of which one was fixed on the sphere while the other exhibited large amplitude motion. Additional two-armed spirals were observed during $15\,000<t<20\,000$. Three of them exhibited little motion during $20\,000<t<25\,000$, and five two-armed spirals were seen on the sphere during $25\,000<t<30\,000$. These five two-armed spirals also exhibited little movement during the final time interval shown in the plot, as indicated by the five more concentrated regions in the corresponding singularity plot [Fig. 3(d), right panel].

In view of the random initial conditions it is interesting to examine the mean number of singularities $\langle n_s(t)\rangle$ versus time determined from an average over initial conditions. Plots of $\langle n_s(t)\rangle$, computed from an average over an ensemble of several initial states, versus time for $\tau=10$ (top line), $\tau=6$ (center line), and $\tau=5$ (bottom line) are shown in Fig. 4 for a sphere with $R=60$. For $\tau=5$, averages were computed using 14 initial states, while 7 initial states were used in each of the other cases. When $\tau=10$ there is no change in the number of singularities after a short transient, and all singularities are associated with rotating single-armed spiral waves (recall top row, Fig. 3). For $\tau=6$ there is a gradual loss of singularities through annihilation events, and all systems were still in a transient state when simulations were stopped. Only isolated rotors and two-armed spirals were observed on the sphere for this value of τ. For $\tau=5$, all 14 initial conditions led to a pair of four-armed spirals (eight singularities in total) for $t>25\,000$, and in one case, the pair of four-armed spirals had already formed at $t\approx 7000$.

In light of the finding that every random initial condition considered (14 in total) led to the same final number of singularities for $\tau=5$, which we classified as four-armed spirals based on a visual inspection of the dynamics of the singularities in the system during the final time interval, we performed a more detailed simulation of the motion of the singularities for $25\,000<t<25\,200$. The result is shown in the Fig. 5(b), where the red trajectory corresponds to the four-armed spiral made up of singularities with $I=-1$ visible in the left view of the sphere [left panel of 5(a)], while the blue trajectory is the motion of the singularities with $I=+1$ making up the four-armed spiral visible in the right view of the sphere [right panel of 5(a)].

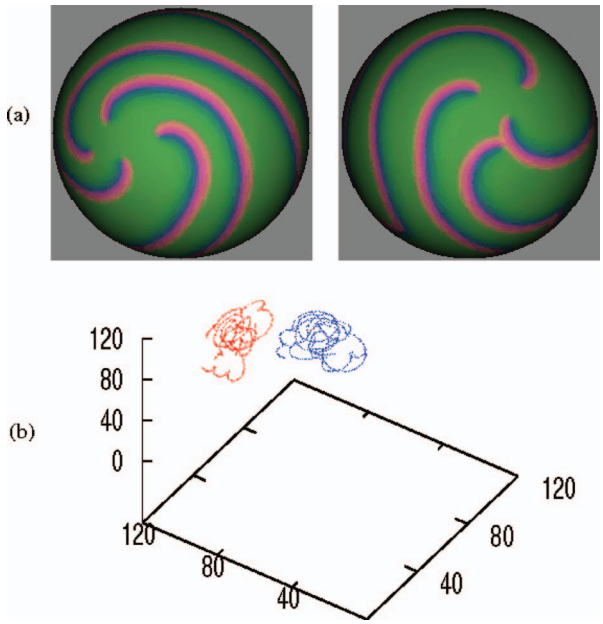

FIG. 5. (Color) (a) Left and right views of a spherical shell with $R=60$ for $\tau=5$, together with a plot of the location of the singularities for every time step in the range $25\,000<t<25\,200$ in (b).

The singularity plot has been rotated in order to more clearly show the meandering of the singularities. In general, one of the four-armed spirals exhibits larger amplitude motion while the other remains more fixed on the sphere. The large amplitude motion is only apparent over time intervals of approximately 5000 time units. In all cases considered the dynamics consisted of four-armed spirals that appeared to execute complex dynamics.

Next, we consider how the average number of singularities as a function of time varies with the radius of the sphere. Figure 6 plots $\langle n_s(t)\rangle$ as a function of time for $R=120$, $R=90$, and $R=60$, for $\tau=5$. For $R=60$ (bottom curve), all realizations evolve to a dynamic state involving one pair of four-armed spirals. For systems that appeared to have reached a steady state in the $R=90$ case (center curve of the figure), some systems evolved to pairs of four-armed spirals, while others led to three-armed spirals (see Fig. 7). The dynamics of the three-armed spirals was similar to that of the four-armed spirals in this medium in that the spirals lie on opposite hemispheres and one spiral exhibits larger amplitude motion than the other. In general, multiarmed spirals typically consisted of three or four arms on spheres with $R=90$, and the remaining singularities were isolated ones. For $R=120$ (top curve of Fig. 6), most systems were still in the

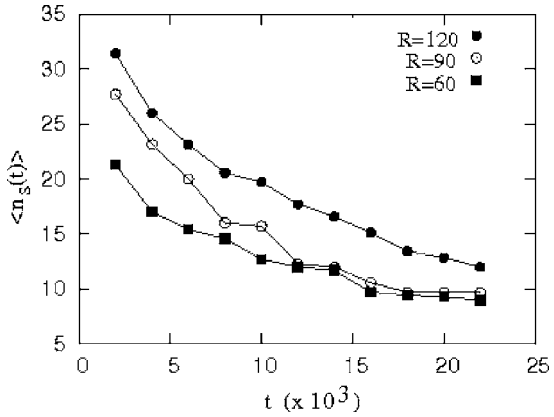

FIG. 6. A plot of $\langle n_s(t) \rangle$ for $\tau=5$ as a function of time for $R=120$ (solid circles), $R=90$ (unfilled circles), and $R=60$ (solid squares).

transient regime when simulations were stopped at $t \approx 22\,000$, although the common trend consisting of a loss of singularities in time is evident in the figure.

B. Comparison with two-dimensional planar media

We now compare the above results with studies of spiral wave dynamics on planar two-dimensional surfaces with no-flux boundary conditions. Such investigations have been carried out by Vasiev *et al.*[15] on small domains for the same FHN model, Eqs. (1) and (2), as a function of k. Simulations of weakly excitable media using a different model have been carried out by Zaritski *et al.*[27] on large domains. In weakly excitable media multiarmed spiral configurations, like those discussed above, have been observed. In large domains, starting from random initial conditions, the system typically self-organizes into a dilute distribution of multiarmed spirals. The number of singularities decreases over time either as a result of collisions with the boundaries or by collisions in which pairs of oppositely rotating spirals collide and annihilate.[27]

We have carried out simulations on the reaction-diffusion equation (1) with FHN kinetics (2) as a function of τ on large (1498×2990 rectangular grids with $\Delta x=0.6$) two-dimensional systems with no-flux boundary conditions to make comparisons of the planar and spherical shell systems for the same model.[61]

For $\tau=8$, initially, recombination and annihilation of singularities occur, but this interaction is short-lived. The remaining singularities survive for long times [see Fig. 8(a)]. For $\tau=7$ [Fig. 8(b)], spiral interactions lead to migration of spirals across the medium, forming small clusters of singularities. Once a cluster is formed, isolated singularities are eventually forced towards the medium boundaries where they are annihilated. For $\tau=6$ [Fig. 8(c)], singularities cluster much earlier, and the annihilation of isolated singularities with the boundaries also occurs more rapidly. For $\tau=5$, the clustering is even faster still, and the removal of isolated singularities occurs very quickly [see Fig. 8(d)].

In general, formation of multiarmed spirals is favored in systems with lower excitability corresponding to smaller val-

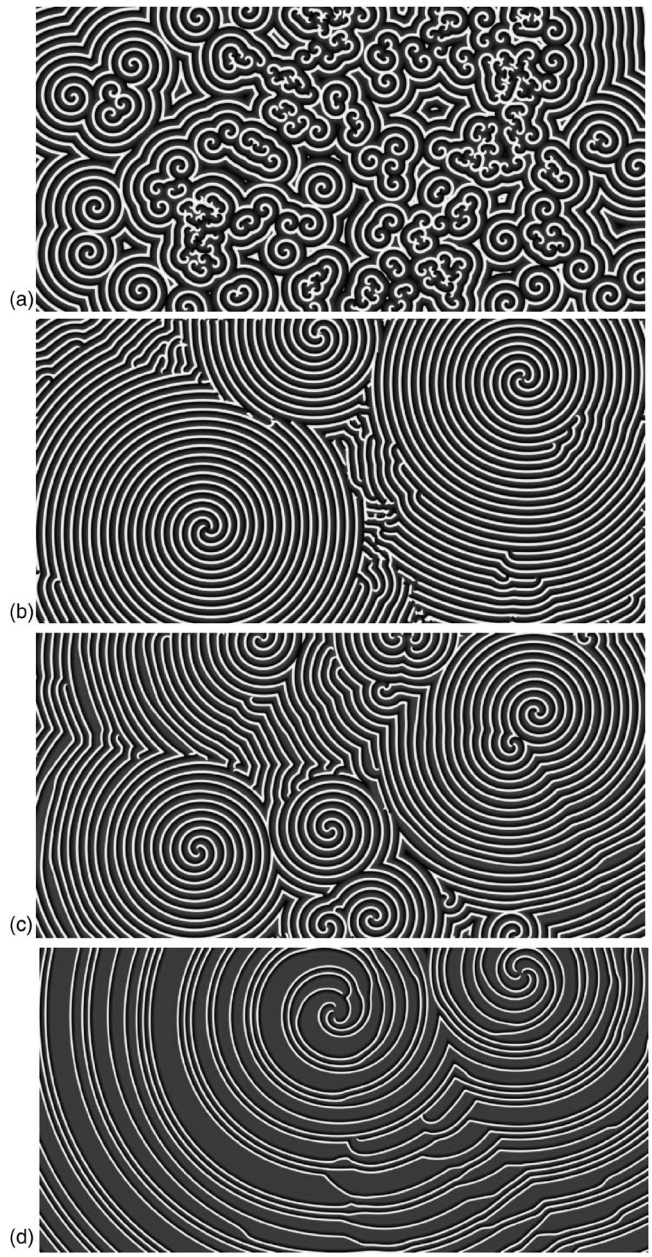

FIG. 8. Spiral configurations on 2D rectangular domains with no-flux boundary conditions for (a) $\tau=8$ at time 7500, (b) $\tau=7$ at time 7500, (c) $\tau=6$ at time 10 000, and (d) $\tau=5$ at time 7500. The formation of several clusters of occurs in all cases except for $\tau=8$. For $\tau=5$, the pair of four-armed spirals appears early ($t \approx 2500$) in the simulation, and persists for the duration of the simulation.

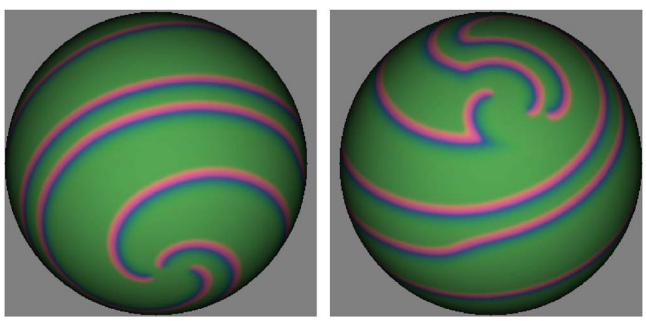

FIG. 7. (Color online) Front and back views of a sphere for $\tau=5$ with $R=90$ showing a pair of three-armed spirals at $t \approx 23\,000$.

ues of $\tau \leq 7$. When multiarmed spirals form, isolated singularities may still persist, primarily in regions between the multiarmed spirals. When τ is sufficiently large, here $\tau \geq 8$, the initially surviving singularities tend to remain fixed in space and do not migrate. In these simulations we observed one-armed spirals for $\tau=8$, three-armed spirals for $\tau=7$, two-armed spirals for $\tau=6$, and four-armed spirals for $\tau=5$.

As noted above, the propensity to form multiarmed spirals is a feature of the reduced excitability of the medium. However, on spherical shells, the sum of the indices must be equal to zero. A multiarmed spiral tends to be paired with another multiarmed spiral with the same number of arms, though the geometries of the two pairs of multiarmed spirals are often not identical. Other spiral geometries could occur based solely on the topological constraints. Hypothetically speaking, a four-armed spiral rotating in one direction could be balanced by two two-armed spirals rotating in the opposite direction. Since there are no boundaries on the sphere, the large number of singularities initially present are removed by annihilation events involving collisions of oppositely rotating spiral waves.

IV. THICK SPHERICAL SHELLS AND SOLID SPHERES

For thick spherical shells, solid spheres or, indeed, any three-dimensional volume of an excitable medium, we must consider the dynamics of scroll waves. For scroll waves the tip of a spiral wave is drawn out to form a vortex filament whose dynamics must be determined. Scroll waves have been observed in a number of different physical systems.[8,62–64]

The filament of the scroll wave is a space curve $\mathbf{R}(s)$ parameterized by the arc length s, $0 \leq s \leq \ell(t)$ with $\ell(t)$ the total length of the filament. The tangent $\hat{\mathbf{t}}(s)$, normal $\hat{\mathbf{n}}(s)$, and binormal $\hat{\mathbf{b}}(s)$ unit vectors to the curve are defined by $\hat{\mathbf{t}}(s)=d\mathbf{R}(s)/ds$, $\hat{\mathbf{n}}(s)=d\hat{\mathbf{t}}/ds/|d\hat{\mathbf{t}}/ds|$ and $\hat{\mathbf{b}}(s)=\hat{\mathbf{t}}(s)\times\hat{\mathbf{n}}(s)$, and satisfy the Frenet-Serret equations,

$$\frac{d\hat{\mathbf{t}}}{ds}=\kappa\hat{\mathbf{n}}, \quad \frac{d\hat{\mathbf{n}}}{ds}=-\kappa\hat{\mathbf{t}}+\tau\hat{\mathbf{b}}, \quad \frac{d\hat{\mathbf{b}}}{ds}=-\tau\hat{\mathbf{n}}, \tag{7}$$

where $\kappa(s)=|d\hat{\mathbf{t}}/ds|$ is the curvature and $\tau(s)=|d\hat{\mathbf{b}}/ds|$ is the torsion.

We must account for the fact that the phase field may twist around the filament; thus, we are led to consider the dynamics of ribbon curves. The local phase of the spiral may be defined as the angle between the unit vector $\hat{\mathbf{V}}$ and a local reference direction. We may choose $\hat{\mathbf{V}}=\hat{\mathbf{b}}\cos\varphi+\hat{\mathbf{n}}\sin\varphi$, where φ is the angle $\hat{\mathbf{V}}$ makes with the binormal.[65] The edges of the ribbon curve are then defined by $\mathbf{X}(s)$ and $\mathbf{X}(s)+\epsilon\hat{\mathbf{V}}(s)$, where ϵ is a small constant. The vector $\hat{\mathbf{V}}$ twists along the filament and the local twist rate is $w(s)=\left(\hat{\mathbf{V}}\times\frac{d\hat{\mathbf{V}}}{ds}\right)\cdot\hat{\mathbf{t}}=\tau(s)+\frac{d\varphi}{ds}$. The twist can be decomposed into the twist of the filament that measures how the binormal twists around the filament, and the ribbon twist, that measures how the ribbon twists around the binormal or Frenet ribbon.

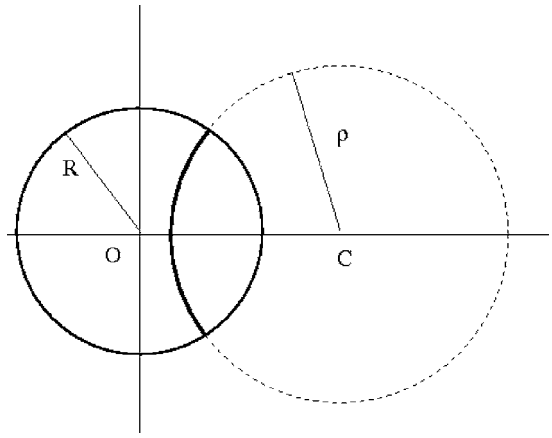

FIG. 9. A scroll wave filament in a solid sphere of excitable medium with radius R in the form of an arc of a circle with radius ρ. This geometry was used to obtain the solution to Eq. (8) given in Eq. (9).

Kinematic descriptions based on the Frenet equations that account for growth or shrinkage of the filament have been constructed.[33,47,65,66] Keener[66] derived the following equation of motion for an untwisted filament in a plane:

$$\frac{d\phi}{dt}=a\kappa, \quad \frac{d\mathbf{R}}{dt}\cdot\hat{\mathbf{b}}=b\kappa, \quad \frac{d\mathbf{R}}{dt}\cdot\hat{\mathbf{n}}=c\kappa, \tag{8}$$

where the coefficients a, b, and c can be determined from the solution of the eigenvalue problem corresponding to the linearized reaction-diffusion equation. The motion of the filament can be resolved into components corresponding to shrinking, $d\mathbf{R}(t,s)/dt\cdot\hat{\mathbf{n}}$, drifting, $d\mathbf{R}(t,s)/dt\cdot\hat{\mathbf{b}}$, and a meandering motion. When $D_u=D_v=D$, $c=D$, and $a=b=0$, an initially planar filament will remain in the same plane at all times and the normal velocity of the filament is proportional to the diffusion coefficient. If the diffusion coefficients are unequal, b is not zero, and a planar filament will not remain planar unless the filament is initially exactly a circle. If a is not zero an untwisted filament will develop twist unless it is exactly circular initially.[66] Some new features enter when spherical shells are considered since the curvature κ depends on the Gaussian curvature Γ of the spherical shell in this case [recall (5)]. Furthermore, a recent generalization of (8) (Ref. 67) extended these ideas to incorporate a dependence of the filament motion itself on the twist of the filament, allowing the study of twist-induced instabilities of the filament.

For FHN kinetics with equal diffusion coefficients, the motion of scroll wave filaments in solid spheres has been investigated.[33] Depending on the parameter values, the filament may form an arc of a circle that shrinks in time, or the filament may meander. When amplitude of meander is small, the filament rapidly adopts the shape of an arc circle with radius $\rho(t)$ and shrinks until it disappears. The relevant geometry is shown in Fig. 9. Solving Eq. (8) for this leads to

$$\rho(t)=R(e^{2c(t_f-t)/R^2}-1)^{1/2}, \tag{9}$$

where t_f is the lifetime of the filament. This result agrees well with simulations of the shrinkage of the filament.[33]

If the parameters of the FHN model change it is possible to enter a regime in which the vortex filament has negative

tension and grows to fill the spherical volume instead of shrinking.[33] This leads to a type of vortex filament turbulence. Such filament turbulence has been studied in 3D cubic or rectangular geometries[68–70] and in 3D heart models.[71–73] In addition to parameter changes, changes in the thickness of the medium can also affect the dynamics of scroll waves in cubic geometries.[74] The full details of the filament dynamics in spherical geometries however, remains to be investigated.

V. CONCLUSIONS

Geometry plays an important role in determining the nature of spiral pattern formation in excitable media. Most excitable media in nature, except in specifically designed laboratory experiments, are not simply planar, but have complex geometries and are inhomogeneous. In order to describe the dynamics of spiral waves in these systems, models must incorporate all of these features. For example, in simulations of cardiac wave propagation that involve realistic heart geometries, the inhomogeneous nature of cardiac tissue and realistic models for cardiac action potentials are now often taken into account.[9]

Studies of spiral wave dynamics on spherical geometries allow one to focus on certain generic aspects of wave propagation on nonplanar surfaces. Two of the most important such aspects are the effects of curvature and the role of boundary conditions on the wave dynamics. Curvature leads to modifications of the wave characteristics and dynamics, including a change in the rotation period of spirals and distinctive dynamics of spirals and vortex filaments. If inhomogeneities in the excitability of the medium are incorporated in the spherical geometry, then new classes of spiral wave patterns are seen, such as source-sink pairs of spirals that are reminiscent of antispirals but have a completely different origin. If the spherical shell is punctured with holes then certain gross features of spiral wave re-entry can be investigated in a simple context. These studies allow one to abstract important features of the pattern formation process that are seen in systems like cardiac tissue which has holes and obstacles due to the presence of valves and veins.

Our simulations on spiral wave dynamics on spherical surfaces as a function of the excitability of the medium revealed a number of interesting features. Spiral tip motion in weakly excitable media often results in waves rotating about a circle of finite radius, and the weaker the excitability, the greater the travel distance of isolated singularities in the medium. This is one of the important distinctions between weakly and highly excitable media. In particular, the effect of the greater travel distance of singularities is to enhance spiral interactions, increasing possible annihilation events and formation of multiarmed spirals if the medium allows it. The additional tendency of waves to lengthen in weakly excitable media until the entire sphere is occupied (recall Fig. 1), leads to a separation of singularities of opposite chirality to opposite hemispheres. The medium excitability controls the extent of each of these factors, which in turn affects the self-organization of the singularities on the sphere.

Through variation of τ in our model we were able to identify and quantify some of the distinctive features that a weakly excitable medium may exhibit compared to a more highly excitable one. Our simulations showed that for stronger excitability corresponding to larger values of τ ($\tau \geq 10$), singularities are essentially fixed in space, while for smaller values of τ, singularities of the same chirality collect on the same hemisphere. This is true regardless of sphere size, and regardless of the value for τ. The type of clusters formed, and the cluster dynamics depend on the value of τ, but an increase in sphere radius does not lead to significant changes.

For $\tau \leq 7$ the interactions among spiral waves on the sphere are similar to those seen in planar media.[15,27] Clustering of singularities leads to formation of multiarmed spirals, some of which rotate stably about fixed cores ($\tau=6$, $\tau=7$), while others exhibit motion across the spherical surface ($\tau=5$). In this last case, we observe long-lived multiarmed spirals with either three or four arms, in which the singular points associated with one chirality form a more localized cluster than those associated with the other chirality. For weakly excitable media, the lack of boundaries in spherical shell geometries leads to a balance between the observed tendency of singularities to separate to opposite hemispheres based on their index, and the tendency of singularities to be expelled from multiarmed spirals formed from singularities with the same index. Such a balance is impossible to obtain in two-dimensional planar geometries, since expelled arms of multiarmed spirals would be lost by collision with the boundaries. The resulting state leads to a very dynamic, yet long-lasting state comprised of four-armed spirals ($\tau=5$, $R=60$).

These results may have implications for drug treatment for cardiac arrhythmias. Arrhythmic drugs act by changing permeability of ionic channels and in this fashion lead to changes in the excitability of cardiac tissue,[75] corresponding in the simplified model to changes in the value of τ. There is a complicated interaction between the value of τ and the geometry of the medium in governing the evolution of spirals and the possible formation of multiarmed spirals. Consequently, it seems reasonable to hypothesize that some antiarrhythmic agents may lead to the formation of multiarmed spirals similar to those observed in some of our simulations. Indeed two-armed spirals have been observed in tissue culture studies of dynamics of cardiac cells.[16]

The theoretical studies of spiral wave dynamics on spherical geometries makes clear that the rich interactions between the geometry of the medium and the excitability of the medium can lead to unexpected self-organization and temporal evolution of spiral waves. Investigation of dynamics in domains of other topologies, such as tori, would be of theoretical interest. Further, these studies underscore the observation that theoretical assessment of the efficacy of drugs used to treat cardiac arrhythmias based on overly simplified analyses, may not be capable of predicting drug effects in the geometrically complex spatially heterogeneous human heart.

ACKNOWLEDGMENT

This work was funded in part by a grant from the Canadian Network of Centers of Excellence on Mathematics of Information Technology and Complex Systems (MITACS).

APPENDIX: EXCITABILITY PARAMETER

The ability of an excitable medium to accommodate spiral waves depends on the medium properties. As the excitability increases, there is a transition from no waves to retracting waves, to rigidly rotating waves, and finally to meandering spirals.[37] If the excitability of the medium is below a minimum value, then waves will retract, while above it, waves lead to re-entry. This minimum excitability can be characterized[37,76,77] by $\Delta_{\min}$,

$$\Delta_{\min} = \left(\frac{R_v(u^+, v^*)}{B a_0^2} \right)^{1/3} D^{1/3}. \tag{A1}$$

Here D is the diffusion constant, $B \approx 0.535$ is a numerical constant determined from a kinematic description for waves in weakly excitable media for which a critical finger (a wave that neither retracts nor leads to re-entry) exists, and R_v is given in Eq. (2). The value for v at which a traveling wave of the system vanishes is denoted by v^*, and points of intersection of $v=v^*$ with the nullcline for u are denoted by u^-, u_0, and u^+ where $u^- < u_0 < u^+$. Since the excitability of the medium for our model is given by $\Delta = v^* - v^{\mathrm{eq}} = v^*$, where $v^{\mathrm{eq}} = 0$ is the equilibrium value for v, we can compare Δ with $\Delta_{\min}$ to predict retracting waves if $\Delta < \Delta_{\min}$, or re-entrant waves if $\Delta > \Delta_{\min}$. To determine $\Delta_{\min}$ we need to compute the parameter a_0 that enters in the expression for the wave speed $c(v)$, $c(v) = a_0(v^* - v)$. For the FHN model v^*, u^+, and a_0 depend on k, l, and a, but are unaffected by changes in τ. However, R_v is inversely proportional to τ, so an increase in τ leads to a decrease in $\Delta_{\min}$ [see (A1)]. Thus, by varying τ for fixed values of the other parameters, we can simulate waves that retract ($\Delta < \Delta_{\min}$), as well as rigid rotors ($\Delta > \Delta_{\min}$).

The parameter a_0 can be determined as follows. Following Tyson and Fife,[78] in seeking plane wave solutions of the reaction-diffusion equation, v is treated as a parameter because it varies slowly. We let $u = u(x - ct)$, where c is the wave speed. Substitution in the reaction-diffusion equation yields the ODE, $D_u u''(z) + c u'(z) + R_u(u(z), v) = 0$, for which the wave speed c vanishes if and only if

$$\int_{u^-}^{u^+} R_u(u, v^*) du = 0. \tag{A2}$$

This equation can be solved to determine v^*.

Next, a piecewise linear approximation to $R_u(u, v^*)$, is made by using the slopes of the curve $R_u(u, v) = 0$ at the points of intersection of $v = v^*$ and the curve. Using implicit differentiation, the slope can be found using $m = -\frac{\partial R_u}{\partial u} \Big/ \frac{\partial R_u}{\partial v}$. Taking m^- to be the slope of $R_u = 0$ at (u^-, v^*), m_0 the slope at (u_0, v^*), and m^+ the slope at (u^+, v^*) leads to the piecewise straight line approximation for $R_u(u, v)$ in the form

$$\begin{aligned} &L_1: m^-(u - u^-) - (v - v^*) \quad \text{for } u \le u_A, \\ &L_2: m_0(u - u_0) - (v - v^*) \quad \text{for } u_A \le u \le u_B, \\ &L_3: m^+(u - u^+) - (v - v^*) \quad \text{for } u \ge u_B, \end{aligned} \tag{A3}$$

where u_A and u_B are the values of u at the points of intersection of L_1 with L_2 and L_2 with L_3, respectively.

Substitution into the ODE, and use of the boundary conditions

$$\lim_{z \to -\infty} u(z) = u^- + (v - v^*)/m^-, \tag{A4}$$

$$\lim_{z \to 0^-} u(z) = u_A = \lim_{z \to 0^+} u(z), \tag{A5}$$

$$\lim_{z \to 0^-} u'(z) = \lim_{z \to 0^+} u'(z), \tag{A6}$$

$$\lim_{z \to z_1^-} u(z) = u_B = \lim_{z \to z_1^+} u(z), \tag{A7}$$

$$\lim_{z \to z_1^-} u'(z) = \lim_{z \to z_1^+} u'(z), \tag{A8}$$

$$\lim_{z \to \infty} u(z) = u^+ + (v - v^*)/m^+, \tag{A9}$$

leads to equations for z_1 and c in terms of v. Solving these numerically for each choice of parameters, allows the determination of the slope that best fits $c(v) = a_0(v - v^*)$. For $k = 4.86$, $l = 1.5$, $a = 0.05$, and $D_u = 1$ a least squares fit of a straight line to ten numerically obtained values for $c(v)$ with v in the range of -0.1 to 0.5 gives $a_0 \approx 3.3$.

[1] *Chemical Waves and Patterns* edited by R. Kapral and K. Showalter (Kluwer, Dordrecht, 1995).
[2] A. L. Belmonte, O. Y. Qi, and J.-M. Flesselles, J. Phys. II **7**, 1425 (1997).
[3] A. N. Zaikin and A. M. Zhabotinsky, Nature (London) **225**, 535 (1970).
[4] A. T. Winfree, Science **175**, 634 (1972).
[5] G. Ertl, Adv. Catal. **37**, 213 (1990).
[6] F. Siegert and C. J. Weijer, Physica D **49**, 224 (1991).
[7] A. Goldbeter, *Biochemical Oscillations and Cellular Rhythms* (Cambridge University Press, Cambridge, 1996).
[8] A. T. Winfree, *When Time Breaks Down: Three Dimensional Dynamics of Electrochemical Waves and Cardiac Arrhythmias* (Princeton University Press, Princeton, 1987).
[9] *Computational Biology of the Heart*, edited by A. V. Panfilov and A. V. Holden (Wiley, Chichester, 1997).
[10] R. A. Gray, A. M. Pertsov, and J. Jalife, Nature (London) **392**, 75 (1998).
[11] F. X. Witkowski, L. J. Leon, P. A. Penkoske, W. R. Giles, M. L. Spano, W. L. Ditto, and A. T. Winfree, Nature (London) **392**, 78 (1998).
[12] J. M. Davidenko, A. V. Pertsov, R. Salomonsz, W. Baxter, and J. Jalife, Nature (London) **355**, 349 (1993).
[13] R. A. Gray and N. Chattipakorn, Proc. Natl. Acad. Sci. U.S.A. **102**, 4672 (2005).
[14] B. T. Ginn and O. Steinbock, Phys. Rev. E **72**, 046109 (2005).
[15] B. Vasiev, F. Siegert, and C. Weijer, Phys. Rev. Lett. **78**, 2489 (1997).
[16] N. Bursac, F. Aguel, and L. Tung, Proc. Natl. Acad. Sci. U.S.A. **101**, 15530 (2004).
[17] R. Feeney, S. Schmidt, and P. Ortoleva, Physica D **2**, 536 (1981).
[18] J. Schütze, O. Steinbock, and S. C. Müller, Nature (London) **356**, 45 (1992).
[19] J. I. Ramos, Chaos, Solitons Fractals **13**, 1383 (2002).
[20] H. Henry, Phys. Rev. E **70**, 026204 (2004).
[21] J. Davidsen, L. Glass, and R. Kapral, Phys. Rev. E **70**, 056203 (2004).
[22] G. Bub, A. Shrier, and L. Glass, Phys. Rev. Lett. **88**, 058101 (2002).
[23] K. H. W. J. ten Tusscher and A. V. Panfilov, Phys. Rev. E **68**, 062902 (2003).
[24] K. H. W. J. ten Tusscher and A. V. Panfilov, Multiscale Model. Simul. **3**, 265 (2005).
[25] B. E. Steinberg, L. Glass, A. Shrier, and G. Bub, Philos. Trans. R. Soc. London, Ser. A **364**, 1299 (2006).
[26] H. Yagisata, M. Mimura, and M. Yamada, Physica D **124**, 126 (1998).
[27] R. M. Zaritski and A. M. Pertsov, Phys. Rev. E **66**, 066120 (2002).
[28] V. A. Davydov and V. S. Zykov, JETP Lett. **76**, 414 (1993).

[29]N. Hartmann, M. Bär, I. G. Kevrekidis, K. Krischer, and R. Imbihl, Phys. Rev. Lett. **76**, 1384 (1996).
[30]O. Blanc, N. Virag, J. M. Vesin, and L. Kappenberger, IEEE Trans. Biomed. Eng. **48**, 1229 (2001).
[31]F. H. Fenton, E. M. Cherry, A. Karma, and W. J. Rappel, Chaos **15**, 13502 (2005).
[32]J. N. Weiss, P. S. Chen, S. F. Lin, H. S. Karegueuzian, H. Hayashi, A. Garfinkel, and A. Karma, Circulation **112**, 1232 (2005).
[33]F. Chavéz, R. Kapral, and L. Glass, Chaos **11**, 757 (2001).
[34]R. FitzHugh, Biophys. J. **1**, 445 (1961).
[35]J. Nagumo, S. Animoto, and S. Yoshizawa, Proc. IRE **50**, 2061 (1962).
[36]This system is a generalization of more commonly studied forms (see Refs. 33, 37, and 38). For $l=\tau$, a linear transformation in u and v exists connecting our system (1) to one with the reactive mechanism $R_u(u,v)=\frac{1}{\epsilon}\left(u-\frac{1}{3}u^3-v\right)$, $R_v(u,v)=\epsilon(u-\alpha v+\beta)$, where the parameters are related by $\alpha=\frac{k(a^2-a+1)}{3\tau}$, $\beta=\frac{(a+1)}{\sqrt{a^2-a+1}}\left[\frac{k(1-2a)(a-2)}{9\tau}+1\right]$ and $\epsilon=\frac{3}{k(a^2-a+1)}$. For all of the simulations discussed here, $l\neq\tau$.
[37]V. Hakim and A. Karma, Phys. Rev. E **60**, 5073 (1999).
[38]A. T. Winfree, Chaos **1**, 303 (1991).
[39]In our simulations the phase Φ was defined by $\Phi(\mathbf{r},t)=\arctan 2(v(\mathbf{r},t)-v_0,u(\mathbf{r},t)-u_0)$, where arctan 2 is the extended arctan function whose range is from $-\pi$ to π, and the point $(u_0,v_0)=(0.3,0.1)$ was chosen to lie inside the orbit of an excitable trajectory in the (u,v) phase space.
[40]A. S. Mikhailov, *Foundations of Synergetics I: Distributed Active Systems* (Springer-Verlag, New York, 1994).
[41]A. T. Winfree and S. H. Strogatz, Physica D **8**, 35 (1982).
[42]L. Glass, Science **198**, 321 (1977).
[43]N. Manz, V. A. Davydov, S. C. Müller, and M. Bär, Phys. Lett. A **316**, 311 (2003).
[44]In the case where $D_v\neq 0$, the velocity curvature relations take on more complicated forms. It has been shown that increasing D_v may result in the transition from planar wave front motion to folded waves, and then to spiral turbulence (see Ref. 45). Furthermore, small perturbations in curvature or external fields may result in dynamic front transitions or nucleation of singularities (see Ref. 46).
[45]V. S. Zykov, A. S. Mikhailov, and S. C. Müller, Phys. Rev. Lett. **81**, 2811 (1998).
[46]C. Elphick, A. Hagberg, and E. Meron, Phys. Rev. E **51**, 3052 (1995).
[47]P. K. Brazhnik, V. A. Davydov, and A. S. Mikhailov, Theor. Math. Phys. **74**, 300 (1988).
[48]A. S. Mikhailov and V. S. Zykov, in *Chemical Waves and Patterns* edited by R. Kapral and K. Showalter (Kluwer, Dordrecht, 1995), p. 119.
[49]P. Grindrod and J. Gomatam, J. Math. Biol. **25**, 597 (1987).
[50]V. A. Davydov and V. S. Zykov, Physica D **49**, 71 (1994).
[51]A. Yu. Abramychev, V. A. Davydov, and V. S. Zykov, Sov. Phys. JETP **70**, 666 (1990).
[52]V. A. Davydov, N. Manz, O. Steinbock, V. S. Zykov, and S. C. Müller, Phys. Rev. Lett. **85**, 868 (2000).
[53]V. Krinsky and K. I. Agladze, Physica D **8**, 50 (1983).
[54]E. A. Ermakova, V. I. Krinsky, A. V. Panfilov, and A. M. Pertsov, Biofizika **31**, 318 (1986).
[55]H. Yagisita, M. Mimura, and M. Yamada, Physica D **124**, 126 (1998).
[56]J. Maselko and K. Showalter, Nature (London) **339**, 609 (1989).
[57]J. Maselko and K. Showalter, React. Kinet. Catal. Lett. **42**, 263 (1990).
[58]V. N. Biktashev and A. V. Holden, Chaos, Solitons Fractals **5**, 575 (1995).
[59]G. Rousseau and R. Kapral, Chaos **10**, 812 (2000).
[60]Unless otherwise stated a spatial discretization of $\Delta x=0.5$ was used in the simulations. The diffusion coefficient $D_v=0$ and $D_u=1$. System sizes and simulation times are reported in the dimensionless units of the FHN reaction-diffusion equation and we have taken $k=4.86$, $l=1.5$, $a=0.05$ and various values of τ.
[61]Using a fixed time step Runge-Kutta method, we performed simulations on 2D sheets of various size for the system (1). A grid size of $\Delta x=0.6$ with time step $\Delta t=0.05$ was used.
[62]O. Steinbock, F. Siegert, S. C. Müller, and C. J. Weijer, Proc. Natl. Acad. Sci. U.S.A. **90**, 7332 (1993).
[63]U. Storb, C. R. Neto, M. Bär, and S. C. Müller, Phys. Chem. Chem. Phys. **5**, 2344 (2003).
[64]V. N. Biktashev, A. V. Holden, S. F. Mironov, A. M. Pertsov, and A. V. Zaitsev, Chaos, Solitons Fractals **13**, 1713 (2002).
[65]M. Tabor and I. Klapper, Nonlinear Sci. Today **4**, 7 (1994); **4**, 12 (1994).
[66]J. P. Keener, Physica D **31**, 269 (1988).
[67]B. Echebarria, V. Hakim, and H. Henry, Phys. Rev. Lett. **96**, 098301 (2006).
[68]S. Alonso, F. Sagués, and A. S. Mikhailov, Science **299**, 1722 (2003).
[69]S. Alonso, R. Kähler, A. S. Mikhailov, and F. Sagués, Phys. Rev. E **70**, 056201 (2004).
[70]M. A. Bray and J. P. Wikswo, IEEE Trans. Biomed. Eng. **49**, 1086 (2002).
[71]A. V. Panfilov, Phys. Rev. E **59**, R6251 (1999).
[72]R. Zaritski, S. F. Mironov, and A. M. Pertsov, Phys. Rev. Lett. **92**, 168302 (2004).
[73]F. H. Fenton, E. M. Cherry, H. M. Hastings, and S. J. Evans, Chaos **12**, 852 (2002).
[74]A. Rusakov, A. B. Medvinsky, and A. V. Panfilov, Phys. Rev. E **72**, 022902 (2005).
[75]*Atrial Arrhythmias: State of the Art*, edited by J. P. DiMarco and E. N. Prystowsky (Futura, New York, 1995), p. 176.
[76]A. Karma, Phys. Rev. Lett. **66**, 2274 (1991).
[77]V. S. Zykov and K. Showalter, Phys. Rev. Lett. **94**, 068302 (2005).
[78]J. J. Tyson and P. C. Fife, J. Chem. Phys. **73**, 2224 (1980).